

Tunable degenerate two-dimensional optomechanical system

Hui Wang, Qifeng Qiao, Chengyu Peng, Ji Xia, and Guangya Zhou*

Department of Mechanical Engineering, National University of Singapore, Singapore 117576

Yan-Jun Zhao

Beijing National Laboratory for Condensed Matter Physics,

Institute of Physics, Chinese Academy of Sciences, Beijing 100190, China

School of Physical Sciences, University of Chinese Academy of Sciences, Beijing 100190, China

Xun-Wei Xu

Department of Applied Physics, East China Jiaotong University, Nanchang, 330013, China

(Dated: October 30, 2018)

We theoretically study photon transmission and mechanical ground state cooling in a two-dimensional optomechanical system that is formed of a suspended graphene sheet on an one-dimensional optomechanical crystal. When the frequencies of graphene resonator and nanobeam resonator(phononic mode of optomechanical crystal) are approximately the same, the Λ -type degenerate four-level system of two-dimensional optomechanics shows two-color optomechanically-induced transparency, and the transparency window could be switched among probe signal's absorption, transparency, and amplification. According to our calculations, the graphene resonator could also effectively assist the ground state cooling of large damping nanobeam resonator in two-dimensional optomechanics.

PACS numbers: 42.79. Gn, 42.50.Wk, 42.50.Lc

I. INTRODUCTION

Cavity optomechanics supports a platform to explore nonlinear and nonclassical effects[1–5]. Large quantities of progresses have been made on the strong optomechanical coupling and mechanical ground state cooling in optomechanics[6–15]. The photonic nonlinear and nonclassical effects induced by optomechanical interaction have been widely studied, such as the OMIT (optomechanically-induced transparency)[16–21], photon blockade[22–29], nonclassical mechanical motion[14, 15, 30–33], optical nonreciprocity[34–37], and so on. The hybrid system of optomechanics and TLS (two-level system) or mechanical resonator also attracts a lot of interest recently [38–43].

The optomechanics have been realized in different systems, such as Whispering-gallery cavity, photonic crystal cavity, microwave circuit, dielectric membrane placed between two high-finesse mirrors, etc.[1, 2, 44]. The graphene sheet has been used to build optomechanics with microwave resonator through radiation pressure interaction[45–48]. Moreover the interaction between photonic crystal cavity and graphene sheet are more interesting, because the photonic cavity might could to detect mechanical motions and nonlinear mechanical properties of graphene sheet with extra high precision[49]. Some recent experiments have shown that the graphene sheet could be used to tune the optical, electrical, and heat transport of photonic crystal cavity[50–55].

However, single layer graphene is almost transparent for visible and infrared lasers[56, 57], so it is difficult to build optomechanics with single layer graphene sheet through radiation pressure type interaction. As verified by the perturbation calculations and recent experiments[50, 51, 58], the graphene sheet leads to frequency shift and an additional damping for photonic cavity mode through gradient force interaction. Thus, the gradient force could be used to build two-dimensional optomechanics consisting of graphene sheet and one-dimensional optomechanical crystal; as for radiation pressure type optomechanical interaction, the multi-layer graphene sheets might be a choice.

With a suspended graphene sheet above an one-dimensional optomechanical crystal, we study photon transmission and mechanical ground state cooling in two-dimensional optomechanics(see Fig.1). The optomechanical type interactions exist between photonic mode and nanobeam resonator(phononic mode of optomechanical crystal) and graphene resonator. Compared with other type multi-mode optomechanics, the steady position of graphene resonator could be easily tuned via the control voltage between graphene sheet and silicon substrate[59, 60]; thus, the damping rate of photonic cavity and graphene-cavity interaction strength could be controlled. Here we mainly focus on the effects of graphene sheet on photon transmission and ground state cooling of nanobeam resonator in one-dimensional optomechanical crystal.

The paper is organized as follows: In Section II, we introduce the two-dimensional optomechanics model. In Section III, we analyze the effects of graphene resonator on photon transmission. In Section IV, we study

* mpezgy@nus.edu.sg

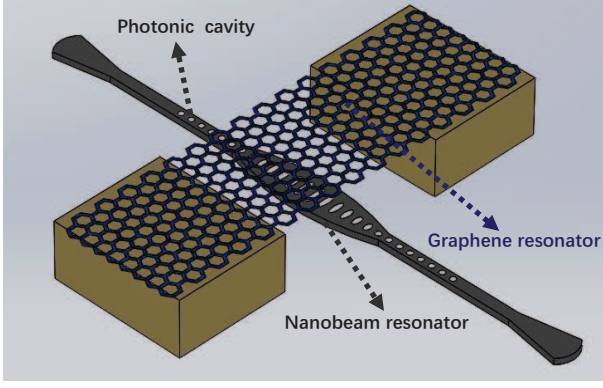


FIG. 1. (Color online) Two-dimensional Optomechanics formed by a suspended Graphene sheet on an one-dimensional optomechanical crystal.

the graphene resonator assisting ground state cooling of nanobeam resonator. In Section V, we conclude this work.

II. TWO-DIMENSIONAL OPTOMECHANICAL MODEL

We study a two-dimensional optomechanical system as shown in Fig. 1, the photonic and phononic modes (nanobeam resonator) of optomechanical crystal interact with each other in the surface parallel with silicon substrate, the graphene sheet interacts with photonic mode in the direction perpendicular to silicon substrate. Thus, the Hamiltonian of free two-dimensional optomechanical system:

$$H_0 = \hbar\omega_a\hat{a}^\dagger\hat{a} + \hbar\omega_b\hat{b}^\dagger\hat{b} + \hbar\omega_c\hat{c}^\dagger\hat{c} + \hbar g\hat{a}^\dagger\hat{a}(\hat{b}^\dagger + \hat{b}) + \hbar\lambda\hat{a}^\dagger\hat{a}(\hat{c}^\dagger + \hat{c}). \quad (1)$$

Here \hat{a} (\hat{a}^\dagger), \hat{b} (\hat{b}^\dagger), and \hat{c} (\hat{c}^\dagger) are annihilation (creation) operators of photon, nanobeam phonon, and graphene phonon, respectively. The ω_a is the resonant frequency of photonic cavity, and ω_b (ω_c) corresponds to vibration frequency of nanobeam (graphene) resonator. The g and λ describe optomechanical interaction strengths of photonic mode with nanobeam and graphene resonators, respectively. The graphene-cavity coupling strength and cavity damping rate could be changed by graphene sheet's steady position which could be easily adjusted by control voltage between graphene and silicon substrate[59, 60].

In a rotating frame defined by an unitary transformation $U_1 = \exp\{\hat{a}^\dagger\hat{a}[g(\hat{b}^\dagger - \hat{b})/\omega_b + \lambda(\hat{c}^\dagger - \hat{c})/\omega_c]\}$, the effective Hamiltonian becomes $H_{eff} = \hbar(\omega_a - \chi_t)\hat{a}^\dagger\hat{a} - \hbar\chi_t\hat{a}^\dagger\hat{a}^\dagger\hat{a}\hat{a} + \hbar\omega_b\hat{b}^\dagger\hat{b} + \hbar\omega_c\hat{c}^\dagger\hat{c}$. The direct photon-phonon interactions disappear in H_{eff} and are replaced by a Kerr nonlinearity term with the coefficient $\chi_t = \chi_b + \chi_c$, where $\chi_b = g^2/\omega_b$ and $\chi_c = \lambda^2/\omega_c$ are the photon nonlinear coefficients induced by nanobeam and graphene res-

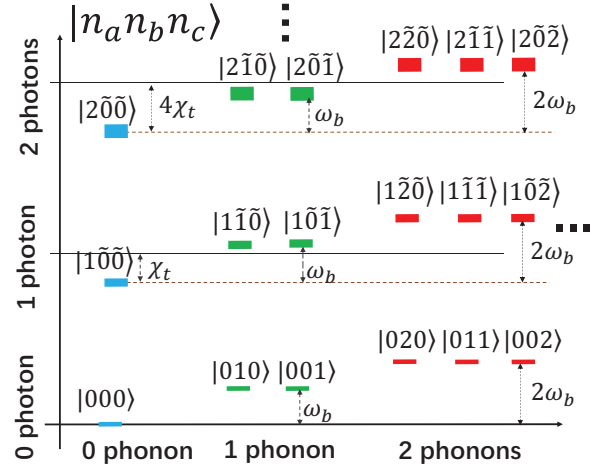


FIG. 2. (Color online) The energy level diagram of two-dimensional degenerate optomechanical system ($\omega_b = \omega_c$). Here $|n_a\rangle$, $|n_b\rangle$, and $|n_c\rangle$ are the Fock states of photon and phonons, while $|\tilde{n}_b\rangle$ and $|\tilde{n}_c\rangle$ correspond to phonon displaced Fock states.

onators, respectively. The energy level structure of two-dimensional optomechanical system could be obtained from H_{eff} as

$$E(n_a, n_b, n_c) = \hbar(\omega_a n_a - \chi_t n_a^2) + \hbar\omega_b n_b + \hbar\omega_c n_c. \quad (2)$$

Here n_a is the cavity photon number, while n_b and n_c are phonon numbers on nanobeam and graphene resonators, respectively. Compared with energy level structure of standard optomechanics[4, 22, 61], the energy levels in two-dimensional optomechanics have an additional mechanical freedom. For degenerate mechanical modes $\omega_b = \omega_c$, the degree of energy level degeneracy could be calculated from Eq. (2) as $n_b + n_c + 1$. The low excitation state energy levels are shown in Fig. 2, the degree of degeneracy for zero phonon state is 1, and it is 2 (or 3) for single (or double) phonon excited states, respectively. From the expression of H_{eff} , the eigenstates of two-dimensional system can be obtained as $|n_a\tilde{n}_b\tilde{n}_c\rangle = U_1|n_a n_b n_c\rangle$, where $|n_i\rangle$ ($i = a, b, c$) are the Fock states of photon and phonons, respectively, while $|\tilde{n}_b(n_a)\rangle$ and $|\tilde{n}_c(n_a)\rangle$ are the phonon displaced Fock states in the case of photon number n_a .

III. TUNABLE PHOTON TRANSMISSION

A. Controllable Photons blockade

The photon blockade in optomechanical system has been widely studied [22–27]. If the photonic cavity is driven by a weak laser field with frequency ω_d and amplitude Ω , that is $H_d = i\hbar[\Omega \exp(-i\omega_d t)\hat{a}^\dagger - h.c.]$. Thus, the Hamiltonian in a rotating frame at driving frequency ω_d , defined by an unitary transformation $U_2 =$

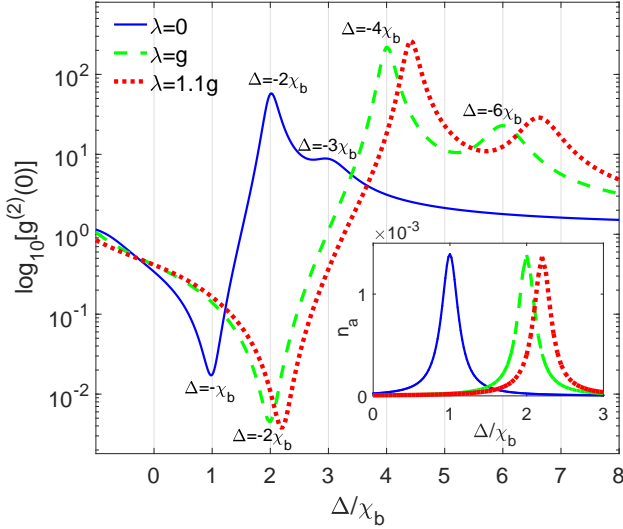


FIG. 3. (Color online) Logarithmic plot of equal-time second-order correlation function $g^{(2)}(0)$ as the function of detuning $\Delta = \omega_d - \omega_a$, with $\omega_b = \omega_c$ and $\chi_b = g^2/\omega_b$. The blue-solid curve describes photon blockade of one-dimensional optomechanics crystal ($\lambda = 0$), while the green-dashed ($\lambda = g$) and red-dotted curves ($\lambda = 1.1g$) correspond to two-dimensional optomechanics. The other parameters are: $\omega_b/(2\pi) = \omega_c/(2\pi) = 100$ MHz, $g/(2\pi) = 20$ MHz, $|\Omega|/(2\pi) = 0.02$ MHz, $\kappa_a/(2\pi) = 1$ MHz, $\kappa_b/(2\pi) = 0.1$ MHz, $\kappa_c/(2\pi) = 1000$ Hz, and $T = 0.01$ K. Inset figure: steady photon numbers.

$\exp(-i\omega_d \hat{a}^\dagger \hat{a} t)$, becomes

$$H_r = -\hbar \Delta \hat{a}^\dagger \hat{a} + \hbar \omega_b \hat{b}^\dagger \hat{b} + \hbar \omega_c \hat{c}^\dagger \hat{c} + \hbar g \hat{a}^\dagger \hat{a} (\hat{b}^\dagger + \hat{b}) + \hbar \lambda \hat{a}^\dagger \hat{a} (\hat{c}^\dagger + \hat{c}) + i\hbar (\Omega \hat{a}^\dagger - \Omega^* \hat{a}). \quad (3)$$

here $\Delta = \omega_d - \omega_a$ is detuning of driving laser and cavity frequency. The photon blockade requires weak driving field ($|\Omega| \ll \kappa_a$) and it is usually described by second-order correlation function which could be defined with density operator as $g^{(2)}(0) = \text{Tr}(\rho \hat{a}^{\dagger 2} \hat{a}^2) / \text{Tr}(\rho \hat{a}^\dagger \hat{a})^2$. The master equations of density operator:

$$\dot{\rho} = \frac{1}{i\hbar} [H_r, \rho] + L_a(\rho) + L_b(\rho) + L_c(\rho). \quad (4)$$

The Lindblad terms in Eq. (4) are: $L_o(\rho) = \frac{\kappa_o}{2} (n_o^T + 1)(2\hat{o}\rho\hat{o}^\dagger - \hat{o}^\dagger\hat{o}\rho - \rho\hat{o}^\dagger\hat{o}) + \frac{\kappa_o}{2} n_o^T (2\hat{o}^\dagger\hat{o}\rho - \hat{o}\hat{o}^\dagger\rho - \rho\hat{o}\hat{o}^\dagger)$, with $o = a, b, c$ corresponding to optical and mechanical variables, respectively. Under weak pumping, the density matrix ρ can be numerically calculated by truncating to limited photon and phonon numbers in Eq. (4) [28, 62–64]. The thermal photon and phonon numbers are defined as $n_o^T = [\exp(\hbar\omega_o/(k_B T)) - 1]^{-1}$ ($o = a, b, c$), with T and k_B are environmental temperature and Boltzmann constants, respectively. Because of the extra high frequency, in this article the thermal photon numbers can be set as zero, that is $n_a^T = 0$.

The numerical calculation results of photon second-order correlation function in degenerate two-dimensional

optomechanical system are shown in Fig. 3. The blue-solid curve describes photon blockade of standard optomechanics, which is equivalent to a large gap between graphene and photonic crystal cavity so that their interaction can be neglected. The peaks and dips in blue-solid curve can be explained analytically as follows. In weak pumping limits $g\sqrt{n_a}|\Omega|/\omega_b \ll \omega_b$ and $\lambda\sqrt{n_a}|\Omega|/\omega_c \ll \omega_c$, the Hamiltonian H_r in Eq. (3), experiencing an unitary transformation U_1 , becomes $H_{wl} \approx -\hbar(\Delta + \chi_t)\hat{a}^\dagger\hat{a} - \hbar\chi_t\hat{a}^\dagger\hat{a}^\dagger\hat{a}\hat{a} + \hbar\omega_b\hat{b}^\dagger\hat{b} + \hbar\omega_c\hat{c}^\dagger\hat{c} + i(\Omega\hat{a}^\dagger - \Omega^*\hat{a})$. There is no direct interaction between photon and phonons in H_{wl} , if we neglect the excitations of phonons [23, 24, 29, 65]; thus, the low excited states wave-function of two-dimensional optomechanics can be assumed as $|\psi\rangle = (A_{000}|0\rangle + A_{100}|1\rangle + A_{200}|2\rangle) \otimes |0_b\rangle \otimes |0_c\rangle$, then the second-order correlation function could be obtained as:

$$g^{(2)}(0) \approx \frac{2|A_{200}|^2}{|A_{100}|^4} \approx 4 \left| \frac{\gamma_a + i2(\Delta - \chi_t)}{\gamma_a + i(\Delta - 2\chi_t)} \right|^2. \quad (5)$$

Equation (5) could be used to explain single-photon blockade dip and two-photon resonant peak in Fig. 3. The dip at $\Delta = -\chi_b$ in blue-solid curve satisfies $g^{(2)}(0) < 1$ and describes single photon blockade of standard optomechanics ($\epsilon = 0$), and the peak at $\Delta = -2\chi_b$ satisfies $g^{(2)}(0) > 1$ and corresponds to two-photon resonant transition. The small peak at $\Delta = -3\chi_b$ corresponds to photon resonant transitions between states $|1, \tilde{n}_b, \tilde{n}_c\rangle$ and $|2, \tilde{n}_b, \tilde{n}_c\rangle$ [23].

The green-dashed and red-dotted curves in Fig. 3 describe photon blockade in two-dimensional optomechanics ($\lambda \neq 0$), which is equivalent to a limited gap between graphene and photonic crystal. In the case of $\lambda = g$ and $\omega_g = \omega_b$, the photon nonlinearity coefficient in green-dashed curve is doubled compared with standard optomechanics (blue-solid curve), that is $\chi_t = 2\chi_b$. So the position of single photon blockade dip (or two-photon resonant peak) shifts to $\Delta = -2\chi_b$ (or $\Delta = -4\chi_b$) in green-dashed curve.

The coupling strength $\lambda = 1.1g$ in the red-dotted curve, the positions of photon blockade dip or multi-photon resonant transition peaks in x -axis deviate from those of green-dashed curve ($\lambda = g$). From above discussions, it is shown that the graphene resonator can be used to tune photon nonlinearity, photon blockade, and photon tunneling in two-dimensional optomechanical system.

B. Optomechanically induced transparency

The OMIT in optomechanical system has been theoretically and experimentally studied [16, 17, 20, 21]. The mechanical mode, TLS, and condensed states coupling to optical or mechanical mode of optomechanics can affect photon transmission and OMIT in optomechanical system [21, 38–42]. If the frequencies of nanobeam and graphene resonators are approximately the same

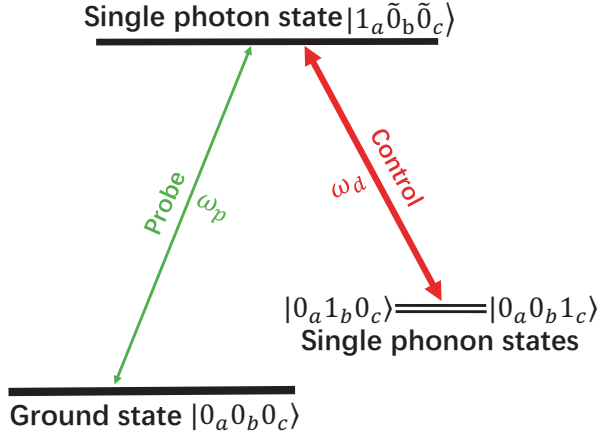


FIG. 4. (Color online) Schematic diagram for the two-dimensional optomechanical system with the driving (control) and probe fields with a single-particle excitation. The vibration frequencies of two mechanical resonators are approximate the same ($\omega_b \approx \omega_c$), the single excitation states form a Λ -type degenerate four-level system, where $|0_a 1_b 0_c\rangle$ and $|0_a 0_b 1_c\rangle$ are single phonon excited states.

($\omega_b \approx \omega_c$), the ground state and single excited states in two-dimensional optomechanical system form a degenerate four-level structure as shown in Fig. 4; thus, the additional photon transition channels $|1_a 0_b 0_c\rangle \leftrightarrow |0_a 0_b 1_c\rangle$ are created by graphene resonator. The energy level structure in Fig. 4 is similar to that of hybrid TLS-optomechanics system, where the TLS splits phonon energy levels and leads to double transparency windows [40].

If the photonic crystal cavity is driven by a strong pumping and a weak probe fields, that is $H_{drive} = i\hbar[\Omega \exp(-i\omega_d t) + \varepsilon \exp(-i\omega_p t)]\hat{a}^\dagger + h.c.$, where Ω (or ω_d) and ε (or ω_p) are the amplitudes (or frequencies) of the driving and probe fields, respectively. In a rotating frame at the driving field frequency ω_d , with the mean field approximation, the steady value equations for photonic and mechanical modes are obtained as

$$\begin{aligned} \langle \dot{\hat{a}} \rangle &= \left(i\Delta - \frac{\kappa_a}{2} \right) \langle \hat{a} \rangle + \Omega + \varepsilon \exp(-i\Delta_p t) \\ &\quad - ig\langle \hat{a} \rangle (\langle \hat{b}^\dagger \rangle + \langle \hat{b} \rangle) - i\lambda\langle \hat{a} \rangle (\langle \hat{c}^\dagger \rangle + \langle \hat{c} \rangle), \\ \langle \dot{\hat{b}} \rangle &= -\left(i\omega_b + \frac{\kappa_b}{2} \right) \langle \hat{b} \rangle - ig\langle \hat{a}^\dagger \rangle \langle \hat{a} \rangle, \\ \langle \dot{\hat{c}} \rangle &= -\left(i\omega_c + \frac{\kappa_c}{2} \right) \langle \hat{c} \rangle - i\lambda\langle \hat{a}^\dagger \rangle \langle \hat{a} \rangle. \end{aligned} \quad (6)$$

where $\Delta_p = \omega_p - \omega_d$ is the detuning between probe and driving fields. When the amplitude of pumping field is much larger than that of the probe field ($|\Omega| \gg |\varepsilon|$), up to the first order small quantity of ε , the solutions of Eqs. (6) can be approximately expanded as $\langle \hat{o} \rangle = O_0 + O_+ \exp(i\Delta_p t) + O_- \exp(-i\Delta_p t)$, with $o = a, b, c$ and $O_{0,\pm} = A_{0,\pm}, B_{0,\pm}, C_{0,\pm}$. Here O_0 and O_\pm are respectively the steady values and first-order responses to weak probe field, and $|O_0| \gg |O_\pm|$. Then the steady value of cavity field can be calculated as $A_0 =$

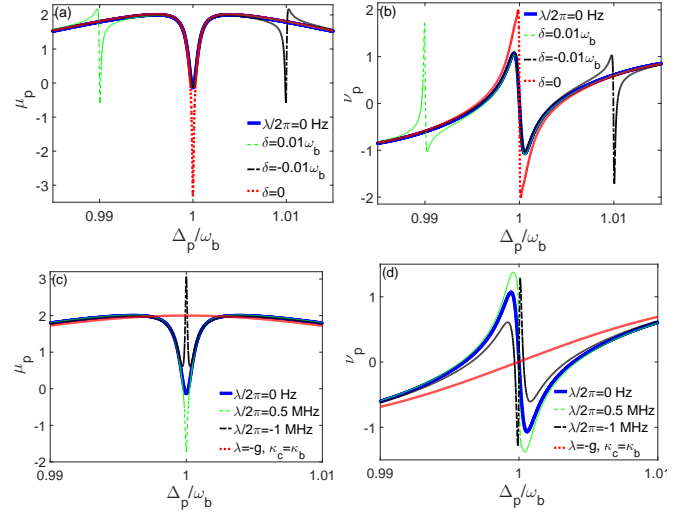


FIG. 5. (Color online) Photon transmission in two-dimensional optomechanics. Probe field's (a) absorption and (b) dispersion for different $\delta = \omega_b - \omega_c$: (i) $\lambda/(2\pi) = 0$ Hz (blue-solid); (ii) $\delta = 0.01\omega_b$ (green-dashed); (iii) $\delta = -0.01\omega_b$ (black-dashed-dotted); (iv) $\delta = 0$ (red-dotted). We specify $\lambda/(2\pi) = 1$ MHz and $\kappa_c/(2\pi) = 0.01$ MHz (except the blue-solid curve). For the same mechanical frequencies ($\omega_b = \omega_c$), the probe field's (c) absorption and (d) dispersion for different λ : (i) $\lambda/(2\pi) = 0$ Hz (blue-solid); (ii) $\lambda/(2\pi) = 0.5$ MHz (green-dashed); (iii) $\lambda/(2\pi) = -1$ MHz (black-dashed-dotted); (iv) $\lambda = -g$ (red-dotted). The mechanical damping rates are the same $\kappa_c = \kappa_b$ in the red-dotted curve, but for other three curves $\kappa_c/(2\pi) = 0.01$ MHz. The other parameters of four figures are: $\omega_b/(2\pi) = 100$ MHz, $\Delta = -\omega_b$, $\kappa_a/(2\pi) = 5$ MHz, $\kappa_b/(2\pi) = 0.06$ MHz, $g/(2\pi) = 4$ MHz, and $|\Omega|/(2\pi) = 10$ MHz.

$\Omega/[\kappa_a/2 - i\Delta + 2ig\text{Re}(B_0) + 2i\lambda\text{Re}(C_0)]$, and mechanical modes' steady values are $B_0 = -ig|A_0|^2/(i\omega_b + \kappa_b/2)$ and $C_0 = -i\lambda|A_0|^2/(i\omega_c + \kappa_c/2)$, respectively.

The first-order small quantity A_- describes probe field's absorption and dispersion in two-dimensional optomechanical system, and it could be calculated from Eqs. (6) as

$$A_- = \frac{\varepsilon}{Q - i\Delta_p - 2igP|A_0|^2 - \frac{4g^2P^2|A_0|^4}{Q - i\Delta_p + 2igP|A_0|^2}}. \quad (7)$$

with $P = \sum_{i=b,c} \theta_i \omega_i / [(\kappa_i/2 - i\Delta_p)^2 + \omega_i^2]$ ($\theta_{b,c} = g, \lambda$), and $Q = \kappa_a/2 - i\Delta + 2ig\text{Re}(B_0) + 2i\lambda\text{Re}(C_0)$. With the input-output relation, the output optical field can be written as $\varepsilon_{out} = (2\kappa_a A_0 - \Omega) + (2\kappa_a A_- - \varepsilon) \exp(-i\Delta_p t) + 2\kappa_a A_+ \exp(i\Delta_p t)$ [17, 68]. Define the quadratures of field as $\varepsilon_T = \mu_p + i\nu_p$, here $\mu_p = \kappa_a(A_-^* + A_-)/\varepsilon$ describes probe field's absorption in two-dimensional optomechanics, while the imaginary part $\nu_p = \kappa_a(A_-^* - A_-)/\varepsilon$ corresponds to dispersion [17].

The effects of mechanical resonators' detuning $\delta = \omega_b - \omega_c$ on transparency window are shown in Figs. 5(a) and 5(b). There is no graphene-cavity interaction in blue-solid curve which describes OMIT of standard optome-

chanics. When the frequencies of two mechanical resonators are the same ($\delta = 0$), the local minimal value within transparency window in red-dotted curve moves down to negative regime, which means that a probe signal propagating in the photonic crystal cavity is not only unabsorbed but also amplified. This phenomenon originates from the additional photon transition channels $|1_a 0_b 0_c\rangle \leftrightarrow |0_a 0_b 1_c\rangle$ that are induced by graphene resonator (see Fig. 4), which enhances the destructive coherent transitions of photons. For a small mechanical detuning $\delta = 0.01\omega_b$ ($-0.01\omega_b$), two transparency windows appear in the green-dashed (black-dashed-dotted) curve, the transparency window at $\Delta_p = \omega_b$ is same as that of standard optomechanics (blue-solid curve) and a new narrow transparency window appears at $\Delta_p = \omega_b - \delta$. This is similar to the double-color transparency window in the TLS-optomechanics coupled systems[40].

For the same mechanical frequencies ($\omega_b = \omega_c$), the effects of graphene-cavity coupling strength λ on transparency window are shown in Figs. 5(c) and 5(d). If the motions of nanobeam and graphene resonators are inphase ($\lambda = g$), the probe signal is amplified in the green-dashed curve. If motions are out of phase $\lambda = -g$, the black-dashed-dotted curve shows that a absorption peak appears within the transparency window of standard optomechanics (blue-solid curve). If the graphene and nanobeam resonators have the same frequencies, damping rates, and optomechanical coupling strengths, but opposite motion phases $\lambda = -g$, the transparency window vanishes in red-dot curve in Fig. 5(c). The destructive coherent transitions induced by two mechanical resonators offset with each other. Through above discussions, it is shown that the graphene resonator can control photon transmission in one-dimensional optomechanics crystal.

IV. GRAPHENE ASSISTING GROUND STATE COOLING

A. Mechanical Spectrum of nanobeam resonator

In the vacuum weak coupling regime $g, \lambda \ll \kappa_a$, the photon operator can be split into $\hat{a} = \alpha + \hat{d}$, with an average coherent amplitude α and a small fluctuation term \hat{d} [6, 66]. From Eq. (3), we can obtain the linearized Heisenberg equations for \hat{d} , \hat{b} , and \hat{c} as follows:

$$\begin{aligned}\dot{\alpha} &= \left(i\Delta - \frac{\kappa_a}{2}\right)\alpha + \Omega, \\ \dot{\hat{d}} &= \left(i\Delta - \frac{\kappa_a}{2}\right)\hat{d} - iG(\hat{b}^\dagger + \hat{b}) - iK(\hat{c}^\dagger + \hat{c}) \\ &\quad + \sqrt{\kappa_a}\hat{a}_{in}(t), \\ \dot{\hat{b}} &= -\left(i\omega_b + \frac{\kappa_b}{2}\right)\hat{b} - i(G^*\hat{d} + G\hat{d}^\dagger) + \sqrt{\kappa_b}\hat{b}_{in}(t), \\ \dot{\hat{c}} &= -\left(i\omega_c + \frac{\kappa_c}{2}\right)\hat{c} - i(K^*\hat{d} + K\hat{d}^\dagger) + \sqrt{\kappa_c}\hat{c}_{in}(t).\end{aligned}\quad (8)$$

with $G = g\alpha$ and $K = \lambda\alpha$. Under strong pumping field, the classical and nonlinear terms $-ig\hat{d}(\hat{b}^\dagger + \hat{b})$, $-i\lambda\hat{d}(\hat{c}^\dagger + \hat{c})$, and $-ig\hat{d}^\dagger\hat{d}$ have been neglected. Thus, the linearized Hamiltonian of two-dimensional optomechanics could be written as $H_L = -\hbar\Delta\hat{d}^\dagger\hat{d} + \hbar\omega_b\hat{b}^\dagger\hat{b} + \hbar\omega_c\hat{c}^\dagger\hat{c} + \hbar(G\hat{d}^\dagger + G^*\hat{d})(\hat{b}^\dagger + \hat{b}) + \hbar(K\hat{d}^\dagger + K^*\hat{d})(\hat{c}^\dagger + \hat{c})$. Here $\hat{o}_{in}(t)$ ($o = a, b, c$) are input noise operators of optical and mechanical modes, respectively; their environmental average values are $\langle\hat{o}_{in}(t)\rangle = 0$, and the nonzero noise input correlation functions are $\langle\hat{o}_{in}(t')\hat{o}_{in}^\dagger(t)\rangle = (n_o^T + 1)\delta(t' - t)$ and $\langle\hat{o}_{in}^\dagger(t')\hat{o}_{in}(t)\rangle = n_o^T\delta(t' - t)$.

With the Fourier transformation, the motion equations in frequency domain are as follows:

$$\begin{aligned}-i\omega\tilde{d}(\omega) &= \left(i\Delta - \frac{\kappa_a}{2}\right)\tilde{d}(\omega) - iG\left[\tilde{b}^\dagger(\omega) + \tilde{b}(\omega)\right] \\ &\quad - iK\left[\tilde{c}^\dagger(\omega) + \tilde{c}(\omega)\right] + \sqrt{\kappa_a}\tilde{a}_{in}(\omega), \\ -i\omega\tilde{b}(\omega) &= -\left(i\omega_b + \frac{\kappa_b}{2}\right)\tilde{b}(\omega) + \sqrt{\kappa_b}\tilde{b}_{in}(\omega) \\ &\quad - i\left[G^*\tilde{d}(\omega) + G\tilde{d}^\dagger(\omega)\right], \\ -i\omega\tilde{c}(\omega) &= -\left(i\omega_c + \frac{\kappa_c}{2}\right)\tilde{c}(\omega) + \sqrt{\kappa_c}\tilde{c}_{in}(\omega) \\ &\quad - i\left[K^*\tilde{d}(\omega) + K\tilde{d}^\dagger(\omega)\right].\end{aligned}\quad (9)$$

Eliminating the variables $\tilde{d}^\dagger(\omega)$, $\tilde{b}(\omega)$, $\tilde{b}^\dagger(\omega)$, $\tilde{c}(\omega)$, and $\tilde{c}^\dagger(\omega)$ in Eqs. (9), with $\tilde{o}^\dagger(\omega) = [\tilde{o}(-\omega)]^*$ ($o = b, c, d$), then $\tilde{b}(\omega)$ can be expressed with input noise operators $\tilde{a}_{in}(\omega)$, $\tilde{b}_{in}(\omega)$, and $\tilde{c}_{in}(\omega)$ [67]. The mechanical spectrum of nanobeam resonator: $S_{bb}(\omega) = \int_{-\infty}^{+\infty} \tilde{b}^\dagger(\omega')\tilde{b}(\omega)d\omega'$ [6, 66]:

$$S_{bb}(\omega) = \frac{\frac{|\alpha|^2}{\kappa_a}\sigma_{opt}(\omega) + \kappa_b\sigma_{th}^{(b)}(\omega) + \kappa_c\sigma_{th}^{(c)}(\omega)}{|N(\omega)|^2}. \quad (10)$$

where

$$\begin{aligned}\sigma_{opt} &= \kappa_a^2 g^2 |\Gamma_b^{-1}(\omega)|^2 |\Gamma_a(\omega)|^2, \\ \sigma_{th}^{(b)} &= n_b^T |\Gamma_b^{-1}(\omega)\Sigma_c(\omega) + i\Sigma(\omega)|^2 + (n_b^T + 1)|\Sigma(\omega)|^2, \\ \sigma_{th}^{(c)} &= \epsilon^2 |\Gamma_b^{-1}(\omega)|^2 |\Sigma(\omega)|^2 \\ &\quad \times [(n_c^T + 1)|\Gamma_c(\omega)|^2 + n_c^T |\Gamma_c(-\omega)|^2], \\ N &= \Gamma_b^{-1}(\omega)[\Gamma_b^{-1}(-\omega)]^*\Sigma_c(\omega) + 2\omega_b\Sigma(\omega).\end{aligned}\quad (11)$$

with $\epsilon = K/G = K^*/G^* = \lambda/g$. The optical and mechanical responsive functions are defined as $\Gamma_a(\omega) = [\kappa_a/2 - i(\omega + \Delta)]^{-1}$, $\Gamma_b(\omega) = [\kappa_b/2 + i(\omega_b - \omega)]^{-1}$, and $\Gamma_c(\omega) = [\kappa_c/2 + i(\omega_c - \omega)]^{-1}$, respectively. The self-energy term of optomechanical crystal is defined as $\Sigma(\omega) = -i|G|^2 [\Gamma_a^{-1}(\omega) - \Gamma_a^{-1}(-\omega)]^*$, which decides frequency shift and extra damping rate of nanobeam resonator in standard optomechanics.

Here σ_{opt} describes contribution of optomechanical interaction between nanobeam resonator and cavity field, $\sigma_{th}^{(b)}$ originates from nanobeam resonator's thermal noises, and $\sigma_{th}^{(c)}$ comes from graphene resonator. Compared with standard optomechanics, an effective amplification factor $\Sigma_c(\omega) = 1 + 2\omega_c\epsilon^2\Sigma(\omega)/[(\kappa_c/2 - i\omega)^2 + \omega_c^2]$,

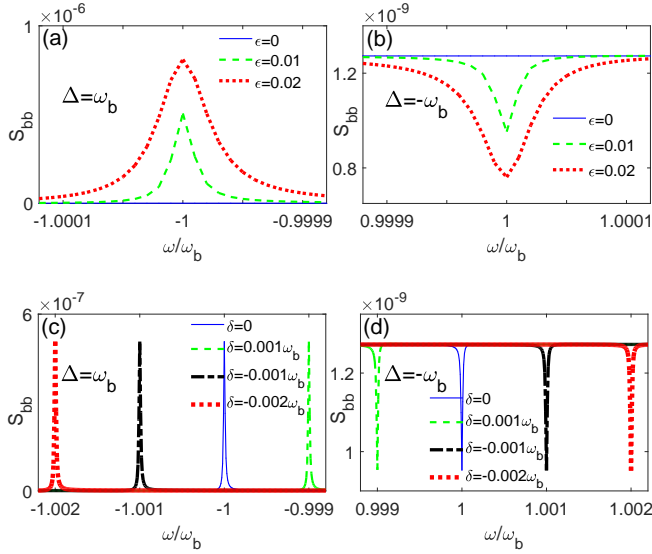


FIG. 6. (Color online) Tunable Mechanical spectrum of nanobeam resonator. The mechanical spectrum under (a) blue-detuning laser and (b) red-detuning laser for different coupling strength λ : (i) $\epsilon = 0$ (blue-solid); (ii) $\epsilon = 0.01$ (green-dashed); (iii) $\epsilon = 0.02$ (red-dotted), here $\delta = 0$. The mechanical spectrum under blue-detuning laser (c) and red-detuning laser (d) for different detuning δ : (i) $\delta = 0$ (blue-solid); (ii) $\delta = 0.001\omega_b$ (green-dashed); (iii) $\delta = -0.001\omega_b$ (black-dashed-dotted); (iv) $\delta = -0.002\omega_b$ (red-dotted), here $\epsilon = 0.01$. The other parameters of four figures are: $\omega_b/(2\pi) = 100$ MHz, $\kappa_a/(2\pi) = 10$ MHz, $\kappa_b/(2\pi) = 10$ MHz, $\kappa_c/(2\pi) = 1000$ Hz, $|G|/(2\pi) = 1.3$ GHz, $n_a^T = 0$, $n_b^T = 100$, and $n_c^T = 100$.

which is induced by graphene resonator, appears in nanobeam resonator's responsive function (see Eq. (11)). The equations $[\Sigma(-\omega)]^* = \Sigma(\omega)$ and $[\Sigma_c(-\omega)]^* = \Sigma_c(\omega)$ have been adopted during the above calculations.

The blue-solid curve in Fig. 6(a) describes mechanical spectrum of standard optomechanics ($\lambda/(2\pi) = 0$ Hz), which has been widely studied in both theories and experiments[1, 4, 6]. If $\epsilon \neq 0$, under blue-detuning driving laser ($\Delta = \omega_b$), the narrow peaks appear at $\omega = -\omega_b$ in green-dashed and red-dotted curves representing the local amplification for mechanical spectrum. The FWHM (Full width at half maximum width) of narrow peak is close to κ_c ($\kappa_c \ll \kappa_b$), which indicates that the narrow peak and dip originate from graphene resonator. For the red-detuning driving laser ($\Delta = -\omega_b$) in Fig. 6(b), a narrow dip appears at $\omega = \omega_b$ in green-dashed and red-dotted curves, which corresponds to local suppression for mechanical spectrum. The dip in red-dotted curve is deeper than that in green-dashed curve, which means that a larger suppression for noise spectrum of nanobeam resonator could be realized with a stronger graphene-cavity coupling. The numerical calculations show that the amplification factor $\Sigma_c(\omega)$ is responsive for the narrow peak or dip in the mechanical spectrum. For a weak graphene-cavity coupling strength, $\Sigma_c(\omega) \approx 1$, the narrow peak or dip will disappear.

The effects of mechanical detuning $\delta = \omega_b - \omega_c$ on mechanical spectrum of nanobeam resonator are shown in Fig. 6(c) (blue-detuning) and 6(d) (red-detuning). For nonzero mechanical detuning ($\delta \neq 0$), under blue detuning driving laser, the x -axis positions of narrow peaks in Fig. 6(c) shift to $\omega = \omega_b + \delta$. For red detuning driving laser in Fig. 6(d), the narrow dips shift to $\omega = \omega_b - \delta$. Thus, we can control the positions of amplification peaks and suppression dips in mechanical spectrum of nanobeam resonator by tuning the frequency of graphene resonator.

B. Dynamical backaction

The optomechanical interaction changes mechanical resonator's frequencies and damping rate[1–4, 6], which can be used for mechanical self-oscillation, phonon laser, mechanical ground state cooling, and so on[14, 15, 54, 69–73]. In this section we discuss the shifts of nanobeam resonator's frequency and damping rate in two-dimensional-optomechanics.

If the frequencies of graphene and nanobeam resonators are approximately the same ($\omega_b \approx \omega_c$), we can obtain from Eqs. (11) that $N(\omega) \approx \Gamma_b^{-1}(\omega)[\Gamma_b^{-1}(-\omega)]^* + 2\omega_b [\epsilon^2\eta(\omega) + 1] \Sigma(\omega)$, with $\eta(\omega) = \Gamma_c(\omega)[\Gamma_c(-\omega)]^* / \{\Gamma_b(\omega)[\Gamma_b(-\omega)]^*\}$. The effective optomechanical self-energy in two-dimensional optomechanics can be defined as $\Sigma_e(\omega) = [\epsilon^2\eta(\omega) + 1]\Sigma(\omega)$. In weak coupling limit $\kappa_b, \kappa_c, \Gamma_{opt} \approx |\alpha|^2/\kappa_a \ll \kappa_a$, the frequency shift and extra damping rate of nanobeam resonator can be defined as $\delta\omega_b^{(o)} = \text{Re}[\Sigma_e(\omega_b)]$ and $\gamma_b^{(o)} = -2\Im[\Sigma_e(\omega_b)]$, respectively. The graphene resonator's frequency shift $\delta\omega_c^{(o)}$ and extra damping rate $\gamma_c^{(o)}$ can be calculated similarly. Because of the symmetry status of two resonators, the $\delta\omega_c^{(o)}$ and $\gamma_c^{(o)}$ can be simply obtained from $\delta\omega_b^{(o)}$ and $\gamma_b^{(o)}$ by interchanging subscript b and c in corresponding expressions, respectively.

The nanobeam resonator's effective frequency $\omega_b^{(e)} = \omega_b + \delta\omega_b^{(o)}$ and damping rate $\kappa_b^{(e)} = \kappa_b + \gamma_b^{(o)}$ in resolved-sideband regime ($\omega_b, \omega_c \gg \kappa_a$) are shown in Figs. 7(a) and 7(b), respectively. The blue-solid curves in Figs. 7(a) and 7(b) correspond to effective frequency and damping rate of standard optomechanics ($\epsilon = 0$). With the increase of graphene-cavity coupling strength, the changes of effective frequency and damping rate become larger in green-dashed and red-dotted curves, which means that graphene resonator can assist mechanical amplification and ground state cooling in two-dimensional optomechanical system.

According to some recent experiments, the coupled mechanical system shows coherent mixing of mechanical modes in bad-cavity limit[74, 75]. The changes of effective frequencies and damping rates for two mechanical resonators in unresolved-sideband regime ($\omega_b, \omega_c \ll \kappa_a$) are shown in Fig. 8, where $\omega_{b,c}^{(e)} = \omega_{b,c} + \delta\omega_{b,c}^{(o)}$ and

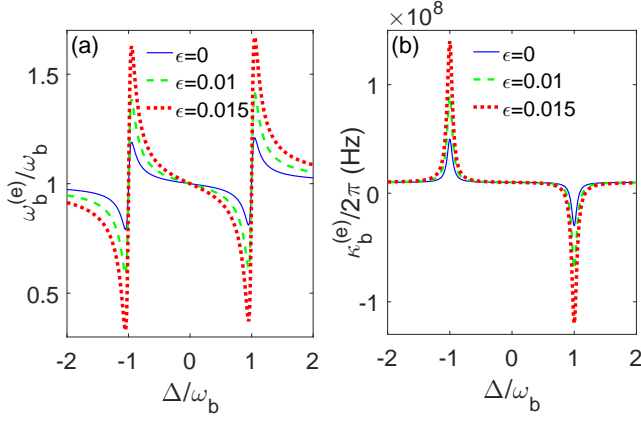


FIG. 7. (Color online) Nanobeam resonator's effective frequency $\omega_b^{(e)} = \omega_b + \delta\omega_b^{(o)}$ and damping rate $\kappa_b^{(e)} = \kappa_b + \gamma_b^{(o)}$ in the resolved-sideband regime. The other parameters are: $\omega_b/(2\pi) = \omega_c/(2\pi) = 100$ MHz, $\kappa_a/(2\pi) = 10$ MHz, $\kappa_b/(2\pi) = 10$ MHz, $\kappa_c/(2\pi) = 1000$ Hz, $|G|/(2\pi) = 10$ MHz, $n_a^T = 0$, $n_b^T = 100$, and $n_c^T = 100$.

$\kappa_{b,c}^{(e)} = \kappa_{b,c} + \gamma_{b,c}^{(o)}$. If $\lambda \ll g$, the changes of two resonators' effective frequencies (Fig. 8(a)) and damping rates (Fig. 8(b)) keep in step with each other. For a large graphene-cavity coupling strength, $\lambda \geq g$, the shifts of effective frequencies (Fig. 8(c)) and damping rates (Fig. 8(d)) in blue-solid and red-dashed curves are the opposite of pace. The damping rates of nanobeam and graphene resonators always have opposite signs in Fig. 8(c), the curves show that if one mechanical resonator is amplified, the other one should be simultaneously cooled. Besides, similar results can also be obtained in resolved-sideband regime. The blue-solid and red-dashed curves in Figs. 8(c) and 8(d) cross with each other, which means that coherent mixing of two mechanical resonators can be realized in two-dimensional optomechanical system with photonic field serving as an intermediary.

C. Ground state cooling of nanobeam resonator

As shown in Fig. 7, the graphene resonator could enhance damping rate of nanobeam resonator, which should make positive contributions to ground state cooling of nanobeam resonator. However, the graphene resonator also introduces a noise term $\sigma_{th}^{(c)}$ in Eq. (10) which makes negative contributions to ground state cooling. The relative sizes of above two terms decide net contributions of graphene sheet on ground state cooling of nanobeam resonator. With the mechanical spectrum in Eq. (10), the phonon number on nanobeam resonator can be obtained as [6, 66]

$$n_m = \int_{-\infty}^{+\infty} \frac{d\omega}{2\pi} S_{bb}(\omega) \quad (12)$$

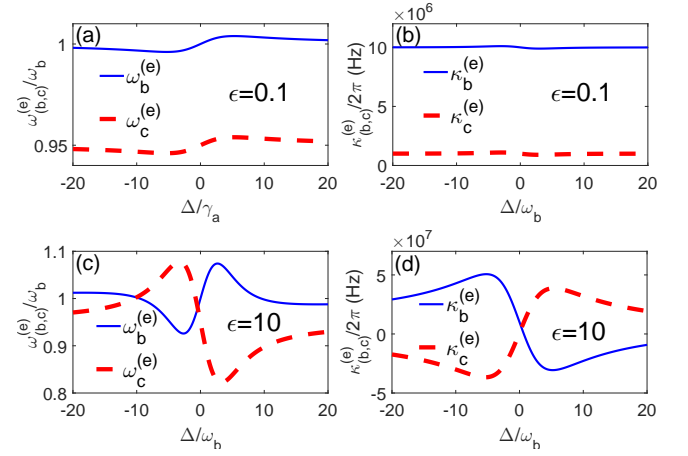


FIG. 8. (Color online) Coherent mechanical mixing in the unresolved-sideband regime. Here (a) and (c) describe effective frequencies ($\omega_{b,c}^{(e)} = \omega_{b,c} + \delta\omega_{b,c}^{(o)}$) of nanobeam (blue-solid) and graphene (red-dashed) resonators, while (b) and (d) correspond to their effective damping rates ($\kappa_{b,c}^{(e)} = \kappa_{b,c} + \gamma_{b,c}^{(o)}$). For (a) and (b) $\epsilon = 0.1$, while $\epsilon = 10$ for (c) and (d). The other parameters of four figures are: $\omega_b/(2\pi) = 100$ MHz, $\omega_c/(2\pi) = 95$ MHz, $\kappa_a/(2\pi) = 1$ GHz, $\kappa_b/(2\pi) = 10$ MHz, $\kappa_c/(2\pi) = 1$ MHz, $|G|/(2\pi) = 10$ MHz, $n_a^T = 0$, $n_b^T = 100$, and $n_c^T = 100$.

The variation of phonon number on nanobeam resonator as increase of graphene-cavity coupling strength is shown in Fig. 9, the value $n_m(\epsilon = 0)$ corresponds to phonon number of standard optomechanics. In blue-solid (or green-dashed) curve of Fig. 9(a), the phonon number of one-dimensional crystal is larger than 1 ($n_m(\epsilon = 0) > 1$); however, the phonon number is quickly suppressed to $n_m < 1$ and reaches ground state as the increase of graphene-cavity coupling strength. For larger cavity damping rate, the suppression ability of nanobeam resonator's phonon number by graphene resonator becomes weaker in green-dashed and red-dotted curves (compared with blue-solid curve).

The ground state cooling of nanobeam resonators in two-dimensional optomechanical system with different damping rates is shown in Fig. 9(b). Compared with small damping rates of blue-solid and green-dashed curves, the phonon number with larger damping rate in red-dotted curve can be more effectively suppressed by graphene resonator. The effects of graphene resonator's damping rate and nanobeam-cavity coupling strength on the ground state cooling of nanobeam resonator are shown in Figs. 9(c) and 9(d), respectively. From above results, it is clear that the graphene resonator can enhance ground state cooling of nanobeam resonator in some parameter regimes, especially for the high damping mechanical resonator.

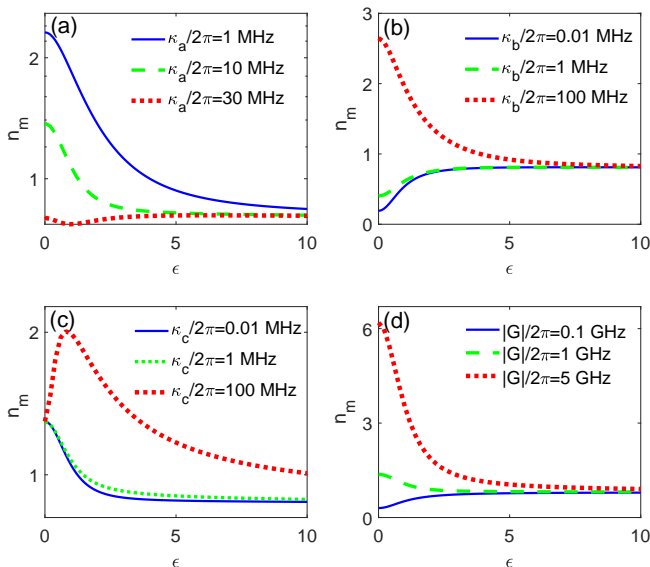


FIG. 9. (Color online) Graphene assisting Ground state cooling of nanobeam resonator. (a) The effects of cavity damping, with $\kappa_b/(2\pi) = 10$ MHz, $\kappa_c/(2\pi) = 0.1$ MHz, and $|G|/(2\pi) = 1$ GHz; (b) The effects of nanobeam damping, with $\kappa_a/(2\pi) = 10$ MHz, $\kappa_c/(2\pi) = 0.1$ MHz, and $|G|/(2\pi) = 1$ GHz; (c) The effects of graphene damping, with $\kappa_a/(2\pi) = 10$ MHz, $\kappa_b/(2\pi) = 10$ MHz, and $|G|/(2\pi) = 1$ GHz; (d) The effects of nanobeam-cavity coupling strength, with $\kappa_a/(2\pi) = 10$ MHz, $\kappa_b/(2\pi) = 10$ MHz, and $\kappa_c/(2\pi) = 0.1$ MHz. The other parameters of four figures are: $\omega_b/(2\pi) = \omega_c/(2\pi) = 100$ MHz, $\Delta = -\omega_b$, $n_a^T = 0$, $n_b^T = 5$, and $n_c^T = 5$.

V. DISCUSSION AND CONCLUSION

We proposed a new type multi-mode optomechanics formed by a graphene resonator coupling to photonic mode of an one-dimensional optomechanical crystal. This kind of two-dimensional system could be experimentally realized by transferring graphene sheets above a released one-dimensional photonic crystal cavity on silicon substrate, and the gap between graphene sheet and photonic cavity is the main difficulty for experimental success. By tuning the control voltage between graphene and silicon substrate, the steady position of graphene sheet can be easily adjusted which can affect the photonic cavity damping and graphene-cavity interaction strength.

We have theoretically studied photon transmission and mechanical ground state cooling in two-dimensional optomechanics. The additional transitions channels induced by graphene resonator could enhance or weaken the destructive coherent transitions of photons, and the probe signal in two-dimensional optomechanics could be switched among absorption, transparency, and amplification by tuning graphene sheet's vibration frequency and steady position.

The graphene resonator could induce narrow amplification peak and suppression dip in the noise spectrum of nanobeam resonator, and affects effective damping rate of nanobeam resonator. According to our numerical calculations, the graphene resonator can assist the ground state cooling of nanobeam resonator in certain parameter regime.

The graphene sheet has some special properties, such as nonlinear mechanical motion and nonlinear mechanical damping, which could be interesting research topics in the future.

VI. ACKNOWLEDGEMENT

Guangya Zhou is supported by MOE Academic Research Fund of Singapore under Grant No. R-265-000-557-112. X.W.X. is supported by the National Natural Science Foundation of China (NSFC) under Grants No.11604096 and the Startup Foundation for Doctors of East China Jiaotong University under Grant No. 26541059. Y.J.Z. is supported by the China Postdoctoral Science Foundation under grant No. 2017M620945.

-
- [1] T. J. Kippenberg and K. J. Vahala, Cavity Optomechanics: Back-Action at the Mesoscale, *Science* **321**, 1172 (2008).
 - [2] M. Eichenfield, J. Chan, R. M. Camacho, K.J. Vahala, and O. Painter, Optomechanical crystals, *Nature* **462**, 78(2009).
 - [3] J.D. Thompson, B. M. Zwickl, A. M. Jayich, F. Marquardt, S. M. Girvin, and J. G. E. Harris, Strong dispersive coupling of a high-finesse cavity to a micromechanical membrane, *Nature* **452**, 72 (2008).
 - [4] M. Aspelmeyer, T. J. Kippenberg, and F. Marquardt, Cavity optomechanics, *Rev. Mod. Phys.* **86**, 1391(2014).
 - [5] M. Poot and H.S.J.van der Zant, Mechanical systems in the quantum regime, *Physics Reports* **511**, 273 (2012).
 - [6] F. Marquardt, J. P. Chen, A. A. Clerk, S. M. Girvin, Quantum Theory of Cavity-Assisted Sideband Cooling of Mechanical Motion, *Phys. Rev. Lett.* **99**, 093902 (2007).
 - [7] I. Wilson-Rae, N. Nooshi, W. Zwerger, and T. J. Kippenberg, Theory of Ground State Cooling of a Mechanical Oscillator Using Dynamical Backaction, *Phys. Rev. Lett.* **99**, 093901 (2007).
 - [8] S. Gröblacher, J. B. Hertzberger, M. R. Vanner, G. D. Cole, S. Gigan, K. C. Schwab, and M. Aspelmeyer, Demonstration of an ultracold micro-optomechanical oscillator in a cryogenic cavity, *Nat. Phys.* **5**, 485 (2009).
 - [9] A. Schliesser, R. Riviere, G. Anetsberger, O. Arcizet, and T. J. Kippenberg, Resolved-sideband cooling of a micromechanical oscillator, *Nat. Phys.* **4**, 415 (2008).
 - [10] J. Chan, T. P. Mayer Alegre, A. H. Safavi-Naeini, J. T. Hill, A. Krause, S. Gröblacher, M. Aspelmeyer, and O. Painter, Laser cooling of a nanomechanical oscillator into its quantum ground state, *Nature* **478**, 89 (2011).

- [11] J. P. Mathew, R. N. Patel, A. Borah, R. Vijay, and M. M. Deshmukh, Dynamical strong coupling and parametric amplification of mechanical modes of graphene drums, *Nature Nanotechnology* **11**, 747 (2016).
- [12] J. B. Clark, F. Lecocq, R. W. Simmonds, J. Aumentado, and J. D. Teufel, Observation of strong radiation pressure forces from squeezed light on a mechanical oscillator, *Nature Physics* **12**, 683 (2016).
- [13] S. Gröblacher, J. B. Hertzberg, M. R. Vanner, G. D. Cole, S. Gigan, K. C. Schwab, and M. Aspelmeyer, *Nat. Phys.* **5**, 485 (2009).
- [14] O. Arcizet, P.-F. Cohadon, T. Briant, M. Pinard, and A. Heidmann, Radiation-pressure cooling and optomechanical instability of a micromirror, *Nature* **444**, 71 (2006).
- [15] Young-Shin Park and Hailin Wang, Resolved-sideband and cryogenic cooling of an optomechanical resonator, *Nature Physics* **5**, 489 (2009).
- [16] S. Weis, R. Riviere, S. Deléglise, E. Gavartin, O. Arcizet, A. Schliesser, T. J. Kippenberg, Optomechanically Induced Transparency, *Science* **330**, 1520 (2010).
- [17] G. S. Agarwal and Sumei Huang, Electromagnetically induced transparency in mechanical effects of light, *Phys. Rev. A* **81**, 041803(R) (2010).
- [18] Sumei Huang and G. S. Agarwal, Electromagnetically induced transparency with quantized fields in optocavity mechanics, *Phys. Rev. A* **83**, 043826 (2011).
- [19] Sumei Huang and G. S. Agarwal, Normal-mode splitting and antibunching in Stokes and anti-Stokes processes in cavity optomechanics: Radiation-pressure-induced four-wave-mixing cavity optomechanics, *Phys. Rev. A* **81**, 033830 (2010).
- [20] A. H. Safavi-Naeini, T. P. Mayer Alegre, J. Chan, M. Eichenfield, M. Winger, Q. Lin, J. T. Hill, D.E. Chang, and O. Painter, Electromagnetically induced transparency and slow light with optomechanics, *Nature* **472**, 69 (2011).
- [21] P. Kómar, S. D. Bennett, K. Stannigel, S. J. M. Habraken, P. Rabl, P. Zoller, and M. D. Lukin, Single-photon nonlinearities in two-mode optomechanics, *Phys. Rev. A* **87**, 013839 (2013).
- [22] P. Rabl, Photon Blockade Effect in Optomechanical Systems, *Phys. Rev. Lett.* **107**, 063601 (2011).
- [23] Xun-Wei Xu, Yuan-Jie Li, and Yu-xi Liu, Photon-induced tunneling in optomechanical systems, *Phys. Rev. A* **87**, 025803 (2013).
- [24] Xun-Wei Xu and Yuan-Jie Li, Antibunching photons in a cavity coupled to an optomechanical system, *J. Phys. B: At. Mol. Opt. Phys.* **46**, 035502 (2013).
- [25] J.Q. Liao, F. Nori, Photon blockade in quadratically coupled optomechanical systems, *Phys. Rev. A* **88** (2), 023853(2013).
- [26] Jie-Qiao Liao and Franco Nori, Single-photon quadratic optomechanics, *Scientific Reports* **4**, 6302 (2014).
- [27] D.W.C. Brooks, T. Botter, S. Schreppler, T.P. Purdy, N. Brahms, and D. M. Stamper-Kurn, Non-classical light generated by quantum-noise-driven cavity optomechanics, *Nature* **488**, 476 (2012).
- [28] T. C. H. Liew and V. Savona, Single Photons from Coupled Quantum Modes, *Phys. Rev. Lett.* **104**, 183601 (2010).
- [29] V. Savona, Unconventional photon blockade in coupled optomechanical systems, arXiv:1302.5937.
- [30] J. D. Teufel, T. Donner, Dale Li, J. W. Harlow, M. S. Allman, K. Cicak, A. J. Sirois, J. D. Whittaker, K. W. Lehnert, and R. W. Simmonds, Sideband cooling of micromechanical motion to the quantum ground state, *Nature* **475**, 359(2011).
- [31] J. Chan, T. P. M. Alegre, A. H. Safavi-Naeini, J. T. Hill, A. Krause, S. Gröblacher, M. Aspelmeyer, and O. Painter, Laser cooling of a nanomechanical oscillator into its quantum ground state, *Nature* **478**, 89 (2011).
- [32] Xun-Wei Xu, Hui Wang, Jing Zhang, and Yu-xi Liu, Engineering of nonclassical motional states in optomechanical systems, *Phys. Rev. A* **88**, 063819 (2013).
- [33] Xun-Wei Xu, Yan-Jun Zhao, and Yu-xi Liu, Entangled-state engineering of vibrational modes in a multimembrane optomechanical system, *Phys. Rev. A* **88**, 022325 (2013).
- [34] Zhen Shen, Yan-Lei Zhang, Yuan Chen, Chang-Ling Zou, Yun-Feng Xiao, Xu-Bo Zou, Fang-Wen Sun, Guang-Can Guo, and Chun-Hua Dong, Experimental realization of optomechanically induced non-reciprocity, *Nature Photonics* **10**, 657 (2016).
- [35] G.A. Peterson, F. Lecocq, K. Cicak, R.W. Simmonds, J. Aumentado, and J.D. Teufel, Demonstration of Efficient Nonreciprocity in a Microwave Optomechanical Circuit, *Phys. Rev. X* **7**, 031001 (2017).
- [36] Kejie Fang, Jie Luo, A. Metelmann, M. H. Matheny, F. Marquardt, A. A. Clerk, and O. Painter, Generalized non-reciprocity in an optomechanical circuit via synthetic magnetism and reservoir engineering, *Nature Physics* **13**, 465 (2017).
- [37] S. Manipatruni, J. T. Robinson, and M. Lipson, Optical Nonreciprocity in Optomechanical Structures, *Phys. Rev. Lett.* **102**, 213903, (2009).
- [38] D. Breyer and M. Bienert, Light scattering in an optomechanical cavity coupled to a single atom, *Phys. Rev. A* **86**, 053819 (2012).
- [39] Peng-Cheng Ma, Jian-Qi Zhang, Yin Xiao, Mang Feng, and Zhi-Ming Zhang, Tunable double optomechanically induced transparency in an optomechanical system, *Phys. Rev. A* **90**, 043825 (2014).
- [40] Hui Wang, Xiu Gu, Yu-xi Liu, A. Miranowicz, F. Nori, Optomechanical analog of two-color electromagnetically induced transparency: Photon transmission through an optomechanical device with a two-level system, *Phys. Rev. A* **90**, 023817(2014).
- [41] Hui Wang, HuiChen Sun, Jing Zhang, and Yu-xi Liu, Transparency and amplification in a hybrid system of the mechanical resonator and circuit QED, *Science China Physics, Mechanics and Astronomy* **55**, 2264 (2012).
- [42] Hui Wang, Xiu Gu, Yu-xi Liu, A. Miranowicz, and F. Nori, Tunable photon blockade in a hybrid system consisting of an optomechanical device coupled to a two-level system, *Phys. Rev. A* **92**, 033806 (2015).
- [43] M. J. Akram, F. Ghafoor, and F. Saif, Electromagnetically induced transparency and tunable Fano resonances in hybrid optomechanics, *J. Phys. B: At. Mol. Opt. Phys.* **48**, 065502 (2015).
- [44] J. D. Thompson, B. M. Zwickl, A. M. Jayich, Florian Marquardt, S. M. Girvin, and J. G. E. Harris, Strong dispersive coupling of a high-finesse cavity to a micromechanical membrane, *Nature* **452**, 72 (2008).
- [45] V. Singh, S. J. Bosman, B. H. Schneider, Y. M. Blanter, A. Castellanos-Gomez and G. A. Steele, Optomechanical coupling between a multilayer graphene mechanical res-

- onator and a superconducting microwave cavity, *Nature Nanotechnology* **9**, 820 (2014).
- [46] P. Weber, J. Guttinger, A. Noury, J. Vergara-Cruz, and A. Bachtold, Force sensitivity of multilayer graphene optomechanical devices, *nature nanotechnology* **7**, 12496 (2016).
- [47] P. Weber, J. Guttinger, I. Tsioutsios, D. E. Chang, and A. Bachtold, Coupling Graphene Mechanical Resonators to Superconducting Microwave Cavities, *Nano Lett.* **14**, 2854 (2014).
- [48] X. Song, M. Oksanen, J. Li, P. J. Hakonen, and M. A. Silanpää, Graphene Optomechanics Realized at Microwave Frequencies, *Phys. Rev. Lett.* **113**, 027404 (2014).
- [49] A. Eichler, J. Moser, J. Chaste, M. Zdrojek, I. Wilson-Rae, and A. Bachtold, Nonlinear damping in mechanical resonators made from carbon nanotubes and graphene, *Nature Nanotechnology* **6**, 339 (2011).
- [50] Xuetao Gan, Kin Fai Mak, Yuanda Gao, Yumeng You, F. Hatami, J. Hone, T. F. Heinz, and D. Englund, Strong Enhancement of Light-Matter Interaction in Graphene Coupled to a Photonic Crystal Nanocavity, *Nano Lett.* **12**, 5626 (2012).
- [51] Huan Li, Y. Anugrah, S. J. Koester, and Mo Li, Optical absorption in graphene integrated on silicon waveguides, *Appl. Phys. Lett.* **101**, 111110 (2012).
- [52] Zhenzhen Xu, Ciyuan Qiu, Yuxing Yang, Qingming Zhu, Xinghong Jiang, Yong Zhang, Weilu Gao, and Yikai Su, Ultra-compact tunable silicon nanobeam cavity with an energy-efficient graphene micro-heater, *Optics Express* **25**, 19479 (2017).
- [53] A. Majumdar, Jonghwan Kim, J. Vuckovic, and Feng Wang, Electrical Control of Silicon Photonic Crystal Cavity by Graphene, *Nano Lett.* **13**, 515 (2013).
- [54] R. A. Barton, I. R. Storch, V. P. Adiga, R. Sakakibara, B. R. Cipriany, B. Ilic, Si Ping Wang, Peijie Ong, P. L. McEuen, J. M. Parpia, and H. G. Craighead, Photo-thermal Self-Oscillation of Graphene Optomechanical Systems, *Nano Lett.* **12**, 4681 (2012).
- [55] Min-Hsiung Shih, Lain-Jong Li, Yi-Chun Yang, Hsiang-Yu Chou, Cheng-Te Lin, and Ching-Yuan Su, Efficient Heat Dissipation of Photonic Crystal Microcavity by Monolayer Graphene, *ACS Nano* **7**, 10818 (2013).
- [56] L. A. Falkovsky, Optical properties of graphene, *J. Phys.: Conf. Ser.* **129**, 012004 (2008).
- [57] R. R. Nair, P. Blake, A. N. Grigorenko, K. S. Novoselov, T. J. Booth, T. Stauber, N. M. R. Peres, A. K. Geim, Fine Structure Constant Defines Visual Transparency of Graphene, *Science* **320**, 1308 (2008).
- [58] J. D. Joannopoulos, S. G. Johnson, J. N. Winn, R. D. Meade, *Photonic Crystals: Molding the Flow of Light*; Princeton University Press: Princeton, NJ, 2008.
- [59] J. S. Bunch, A. M. van der Zande, S. S. Verbridge, I. W. Frank, D. M. Tanenbaum, J. M. Parpia, H. G. Craighead, P. L. McEuen Bunch, Electromechanical Resonators from Graphene Sheets, *Science* **315**, 490 (2007).
- [60] Changya Chen, S. Rosenblatt, K. I. Bolotin, W. Kalb, P. Kim, I. Kymissis, H. L. Stormer, T. F. Heinz, and J. Hone, Performance of monolayer graphene nanomechanical resonators with electrical readout, *nature nanotechnology* **4**, 861 (2009).
- [61] A. Nunnenkamp, K. Børkje, and S. M. Girvin, Single-Photon Optomechanics, *Phys. Rev. Lett.* **107**, 063602 (2011).
- [62] S. M. Tan, A computational toolbox for quantum and atomic optics, *J. Opt. B* **1**, 424 (1999).
- [63] J. R. Johansson, P. D. Nation, and F. Nori, QuTiP: An opensource Python framework for the dynamics of open quantum systems, *Comput. Phys. Commun.* **183**, 1760 (2012).
- [64] J. R. Johansson, P. D. Nation, and F. Nori, QuTiP 2: A Python framework for the dynamics of open quantum systems, *Comput. Phys. Commun.* **184**, 1234 (2013).
- [65] M. Bamba, A. Imamoglu, I. Carusotto, and C. Ciuti, Origin of strong photon antibunching in weakly nonlinear photonic molecules, *Phys. Rev. A* **83**, 021802(R) (2011).
- [66] A. H. Safavi-Naeini, J. Chan, J. T. Hill, S. Gröblacher, Haixing Miao, Yanbei Chen, M. Aspelmeyer, and O. Painter, Laser noise in cavity-optomechanical cooling and thermometry, *New J. Phys.* **15**, 035007 (2013).
- [67] S. Mancini and P. Tombesi, Quantum noise reduction by radiation pressure, *Phys. Rev. A* **49**, 4055 (1994).
- [68] C. W. Gardiner and P. Zoller, *Quantum Noise*. Springer, 2004.
- [69] Yan-Lei Zhang, Chang-Ling Zou, Chuan-Sheng Yang, Hui Jing, Chun-Hua Dong, Guang-Can Guo, Xu-Bo Zou, Phase-Controlled Phonon Laser, *arXiv:1706.02097*.
- [70] D. Navarro-Urrios, N. E. Capuj, M. F. Colombano, P. D. García, M. Sledzinska, F. Alzina, A. Griol, A. Martinez, and C. M. Sotomayor-Torres, Nonlinear dynamics and chaos in an optomechanical beam, *Nature Communications* **8**, 14965 (2017).
- [71] U. Kemiktarak, M. Durand, M. Metcalfe, and J. Lawall, Mode Competition and Anomalous Cooling in a Multimode Phonon Laser, *Phys. Rev. Lett.* **113**, 030802 (2014).
- [72] I. S. Grudinin, H. Lee, O. Painter, and K. J. Vahala, Phonon Laser Action in a Tunable Two-Level System, *Phys. Rev. Lett.* **104**, 083901 (2010).
- [73] Hui Wang, Zhixin Wang, Jing Zhang, Ş. K. Özdemir, Lan Yang, and Yu-xi Liu, Phonon amplification in two coupled cavities containing one mechanical resonator, *Phys. Rev. A* **90**, 053814 (2014).
- [74] Qiang Lin, J. Rosenberg, D. Chang, R. Camacho, M. Eichenfield, K. J. Vahala and O. Painter, Coherent mixing of mechanical excitations in nano-optomechanical structures, *Nature Photonics* **4**, 236 (2010).
- [75] Xingwang Zhang, Tong Lin, Feng Tian, Han Du, Yongchao Zou, Fook Siong Chau, and Guangya Zhou, Mode competition and hopping in optomechanical nanoscillators, *Appl. Phys. Lett.* **112**, 153502 (2018).